AD_____

AWARD NUMBER: W81XWH-08-1-0716

TITLE: Development of Lipid-Based Nanoparticles for In Vivo Targeted Delivery of Imaging Agents into Breast Cancer Cells

PRINCIPAL INVESTIGATOR: Anatoliy V. Popov, Ph.D.

CONTRACTING ORGANIZATION: University of Pennsylvania
Philadelphia, PA 19107

REPORT DATE: October 2009

TYPE OF REPORT: Annual

PREPARED FOR: U.S. Army Medical Research and Materiel Command
Fort Detrick, Maryland 21702-5012

REPORT DOCUMENTATION PAGE

Form Approved
OMB No. 0704-0188

1. REPORT DATE	2. REPORT TYPE	3. DATES COVERED
1 October 2009	Annual	15 Sep 2008 – 14 Sep 2009

4. TITLE AND SUBTITLE

Development of Lipid-Based Nanoparticles for In Vivo Targeted Delivery of Imaging Agents into Breast Cancer Cells

5a. CONTRACT NUMBER

5b. GRANT NUMBER
W81XWH-08-1-0716

5c. PROGRAM ELEMENT NUMBER

6. AUTHOR(S)

Anatoliy V. Popov, Ph.D.

E-Mail: avpopov@mail.med.upenn.edu

5d. PROJECT NUMBER

5e. TASK NUMBER

5f. WORK UNIT NUMBER

7. PERFORMING ORGANIZATION NAME(S) AND ADDRESS(ES)

University of Pennsylvania
Philadelphia, PA 19107

8. PERFORMING ORGANIZATION REPORT NUMBER

9. SPONSORING / MONITORING AGENCY NAME(S) AND ADDRESS(ES)
U.S. Army Medical Research and Materiel Command
Fort Detrick, Maryland 21702-5012

10. SPONSOR/MONITOR'S ACRONYM(S)

11. SPONSOR/MONITOR'S REPORT NUMBER(S)

12. DISTRIBUTION / AVAILABILITY STATEMENT
Approved for Public Release; Distribution Unlimited

13. SUPPLEMENTARY NOTES

14. ABSTRACT

Breast cancer represents a unique disease in oncology, in that specific markers have been identified and are routinely used for diagnosis and targeted therapy. Targeted delivery of a combined imaging and therapy agent to cancer cells is an avenue to develop a new generation of effective and selective anticancer agents. The goal of this proposal is to develop novel nanoparticles for in vivo breast cancer targeting. The nanoparticles consist of a cholesterol ester core surrounded with a lipid monolayer shell containing an imaging agent and metal chelating groups that can attach proteins of interest through specific His6 tagging. Thus far we have synthesized nanoparticle building blocks as well as imaging agents; optimized nanoparticles core composition that provides the minimum nanoparticles size of 8 nm; found out that shell loaded image is much more effective than core loaded one. We have prepared a number of lipid nanoparticles with His6-tagged targeting proteins, which were successfully tested in vitro for optical imaging of model cell lines. We have developing lipid nanoparticles, which are loaded with optical and MR imaging agents and coordinationally bound with different ligands for targeting HER-2/neu on breast cancer cells. In near future we will test these nanoparticles with SK-BR-3 (HER-2/neu+) and MDA-MD-468 (HER-2/neu-) breast cancer cell lines.

15. SUBJECT TERMS
Breast Cancer, Nanoparticles, Near Infrared Optical Imaging, Magnetic Resonance Imaging, Targeted Delivery, Porphyrins, Photodynamic Therapy, Epidermal Growth Factor Receptor, HER-2/neu

16. SECURITY CLASSIFICATION OF:			17. LIMITATION OF ABSTRACT	18. NUMBER OF PAGES	19a. NAME OF RESPONSIBLE PERSON
a. REPORT	b. ABSTRACT	c. THIS PAGE			19b. TELEPHONE NUMBER *(include area code)*
U	U	U	UU	21	USAMRMC

Standard Form 298 (Rev. 8-98)
Prescribed by ANSI Std. Z39.18

Table of Contents

1. Introduction

Targeted delivery of imaging and therapeutic agents to cancer cells is thought to be effective diagnostic and therapeutic modalities to diagnose and treat breast cancer[1,2]. Application of lipid-based platform for the delivery appears to be one of the most promising approaches due to a low toxicity and biodegradable nature of this platform[3]. Thus far, liposomes have been extensively utilized to develop various delivery systems. There are several problems, however, with the liposome delivery system that needs to be overcome to improve the specificity and effectiveness of the delivery[4].

First, liposomes that are currently available have relatively large size, i.e., 100-200 nm, and can be effectively captured by reticuloendothelial system decreasing the specificity and effectiveness of targeting.

Second, incorporation of ligands into the liposomes that determine the specificity of the targeting often requires chemical modification of these ligands that could result in loss of ligands biological activity.

Third, ligands that are often used for specific targeting of liposomes are not natural ligands of receptors of interest and, therefore, less likely would induce endocytosis; meanwhile, the latter facilitates both specificity and effectiveness of the targeting. In addition, natural ligands are less likely to be immunogenic as opposed to antibodies that could elicit unwanted immune response.

We propose to developed novel lipid-based nanoparticles that have size around 10 nm and possess next features:

(i) hydrophobic core surrounded by lipid based monolayer that results in formation of biodegradable nanoparticles with increased stability;

(ii) conjugation of imaging and therapeutic agents with lipid components of the nanoparticle core that result in stable entrapment of the agents leading to increased specificity of targeted delivery;

(iii) use of ligands for targeting of Human epidermal growth factor receptor 2 (HER-2/neu) as well as other receptors, which are overexpressed on breast cancer cells, that induce rapid endocytosis of ligated receptors increasing the specificity of targeting delivery of imaging and therapeutic agents into the tumor cells.

In this grant, we have proposed to demonstrate in proof-of principle the fabrication feasibility of such universal multimodal lipid-based biodegradable platform. We will measure the size, stability and *in vitro* specificity of the nanoparticles. These data will be used for submission a grant to further improvement of the nanoparticles and study the nanoparticle specificity and effectiveness of the delivery of imaging and therapeutic agents *in vivo*.

2. Body

2.1. Research Overview

Targeted delivery of imaging and therapeutic agents to cancer or infected cells is one of the most effective diagnostic and therapeutic modalities to treat human diseases. Rapid development of nanotechnology opens new possibilities to design various nanoplatforms to combine imaging and/or therapeutic agents for targeting delivery. The most widely used nanoplatforms thus far are semiconductor quantum dots, iron oxide and gold nanocrystals, dendrimers or small sized uniform polymer, and various lipid-based nanoparticles[2,5]. A common problem in developing the nanoplatforms is *in vivo* nanoparticle biodegradability, which is related to particles short- and long-term toxicity. The lipid-based nanoparticles are an excellent example of non-toxic and completely biodegradable nanoparticles.

To develop universal multimodal lipid-based nanoparticles that could carry imaging compounds for visualization cancer cells, we have opted to create lipid-based nanoparticles composed of hydrophobic cholesterol esters core[6] and PEGylated shell lipids. While the shell is designed to carry imaging agents, it is primarily made to contain metal-chelating groups that attached targeting molecules to the nanoparticles through interaction with targeting molecule His-tag. The core stabilizes nanoparticles and can also bear imaging agents. Imaging agents are being synthesized as Near Infrared (NIR) dye-lipid conjugates[7]. The nanoparticles are to be conjugated with ICAM-1 ligand for integrin and used to investigate their binding to target cell surface and stability in serum containing media. These data will provide information about potential of the nanoparticles as *in vivo* imaging agent.

The research therefore consists of three major parts:

(i) Synthesis of imaging agents (NIR dye-lipid conjugates and Gd-lipid chelates) and nanoparticles building block (core component);

(ii) Nanoparticles assembly and size measurements;

(iii) *In vitro* imaging of model cells with the lipid nanoparticles and studying their stability.

The project is ongoing and the obtained results presented and discussed below.

2.2. Results

2.2.1. Synthesis of imaging agents

Synthesis of pyropheophorbide *a* (Pyro).

Synthesis of Pyropheophorbide *a* (λ_{abs} 660 nm, λ_{em} 725 nm) from *Spirulina Pacifica* algae is presented in Scheme 1.

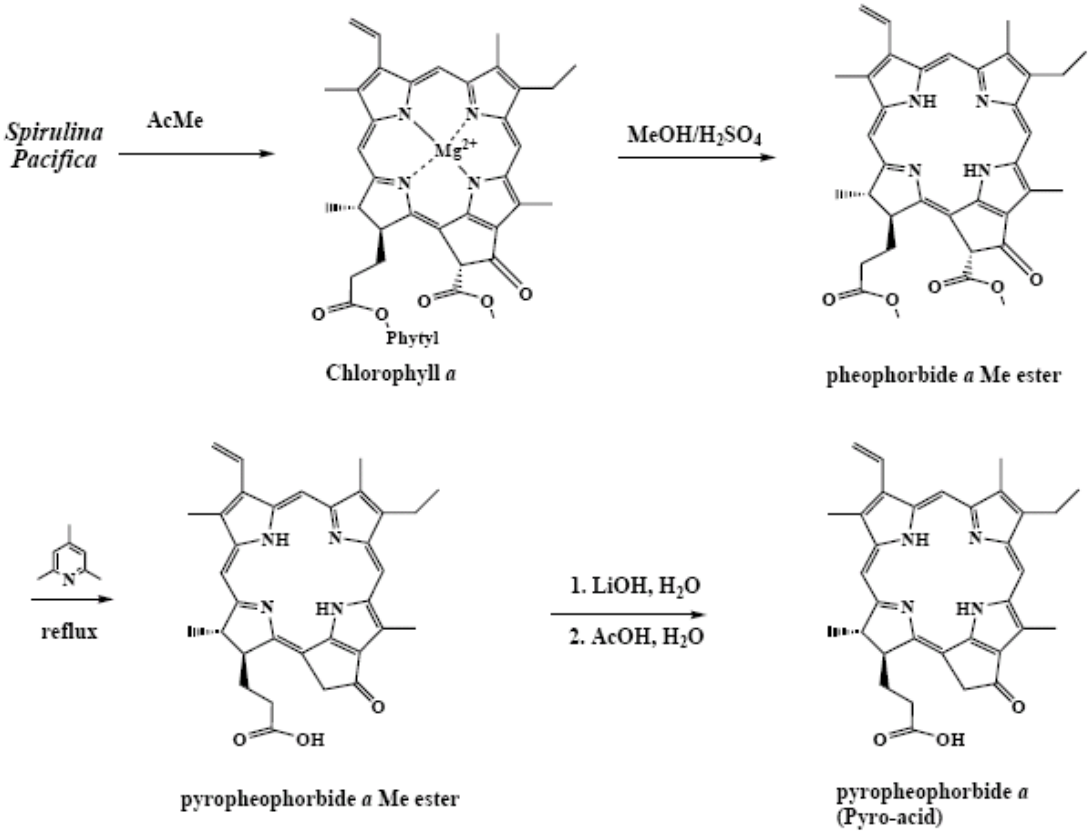

Scheme 1. Synthesis of pyropheophorbide *a*

1.5 g of Pyro-acid was obtained from 1.5 kg of Spirulina Pacifica. Pyro-acid was used in syntheses of imaging components both for the nanoparticles core (Pyro-CE-OA) and shell Pyro-PE (*vide infra*).

Synthesis of 1-palmytoyl-2-pyropheophorboyl-*sn*-glycero-3-phosphatidyl-ethanol amine (Pyro-PE)

Synthesis of Pyro-PE from N-Boc protected *Lyso*-PE and Pyro acid is depicted in Scheme 2. (This is an original synthesis. The details will be published in article[7], which is under preparation for the Journal of the American Chemical Society)

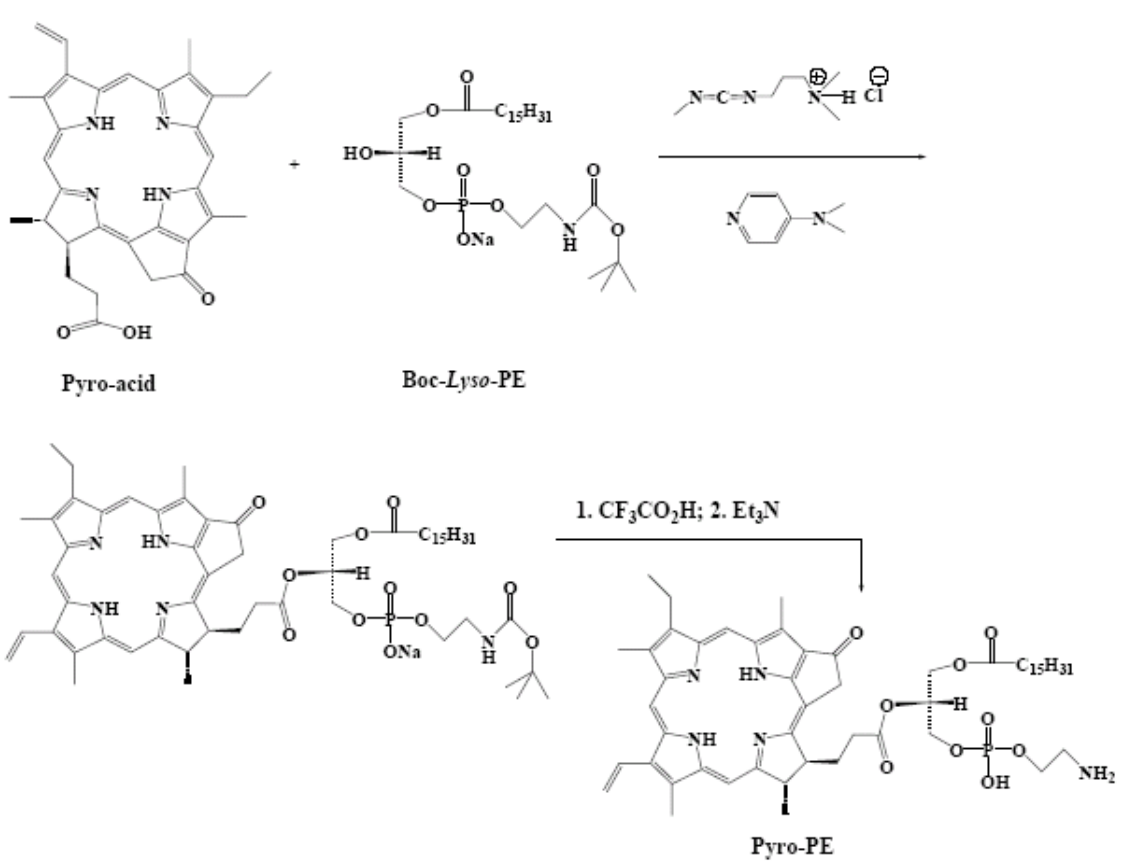

Scheme 2. Synthesis of 1-palmytoyl-2-pyropheophorboyl-*sn*-glycero-3-phosphatidyl-ethano amine (Pyro-PE)

40 mg of Pyro-PE was obtained and used for shell image loading of the lipid nanoparticles.

Synthesis of 5-Androsten-17β-pyropheophorboyl-amino-3β-yl Oleate (Pyro-CE-OA)

We have developed a completely new two-step synthesis of 5-Androsten-17β-pyropheophorboyl-amino-3β-yl Oleate (Pyro-CE-OA). This synthetic pathway is presented in Scheme 3.

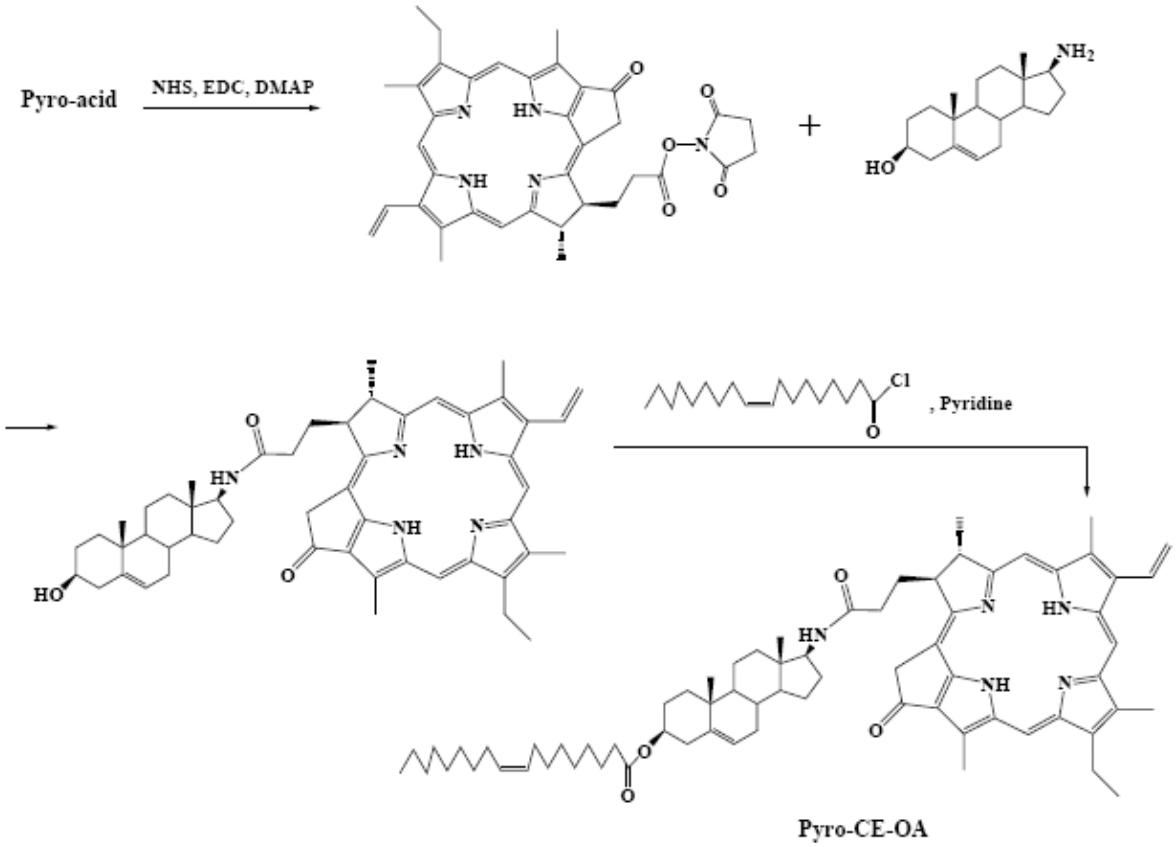

Scheme 3. Synthesis of 5-Androsten-17β-pyropheophorboyl-amino-3β-yl Oleate (Pyro-CE-OA)

140 mg of Pyro-CE-OA was obtained and used for core image loading of the lipid nanoparticles. ^{1}H NMR ($CDCl_3$): 9.37, 9.33, and 8.55 (each s, 1H, 5-H, 10-H, and 20-H of pyro); 8.00 (dd, J = 17.7, 11.4 Hz, 1H, 3^1-CH=CH_2 of Pyro); 6.28 (d, J = 17.7 Hz, 1H, *trans*-3^2-CH=CH_2 of pyro); 6.17 (d, J = 11.4 Hz, 1H, *cis*-3^2-CH=CH_2 of pyro); 5.31 (m, 3H, 2 x vinyl-H and 6-H of oleate), 5.23 (ABX, 2H, 13^2-CH_2 of pyro); 5.02 (m, 1H, N-H of cholesterol), 4.55 (m, 2H, 18-H of pyro, 3-H of cholesterol); 4.35 (m, J = 7.8 Hz, 1H for 17-H of pyro); 3.75 (m, 1H, 17-H of cholesterol), 3.63 (q, J = 7.4 Hz, 2H, 8-C$H_2$$CH_3$ of Pyro); 3.47, 3.46 and 3.23 (each s, 3H, 12-CH3, 2-CH_3 and 7-CH_3 of pyro); 2.71 and 2.46 (each m, 2H, for 2 x 17^1-H and 2 x 17^2-H of pyro); 2.22 (m, 6H of cholesterol oleate), 2.10-1.75 (m, 11H of cholesterol oleate), 1.70-0.95 (m, 39H of cholesterol oleate), 1.82 (d, J = 7.2 Hz, 3H, 18-CH_3 of Pyro); 1.65 (t, J = 8.3 Hz, 3H, 8-CH_2CH_3 of pyro), 0.88 (m, 6H, 19-CH_3 of cholesterol and terminal CH_3 of oleate), 0.32 (s, 3H, 18-CH_3 of cholesterol).

Synthesis of diethylenetriamine pentaacetic acid bis-stearylamide Gagolinium salt monohydrate (DTPA-DSA-Gd)

Synthesis of diethylenetriamine pentaacetic acid bis-stearylamide (DTPA-DSA).

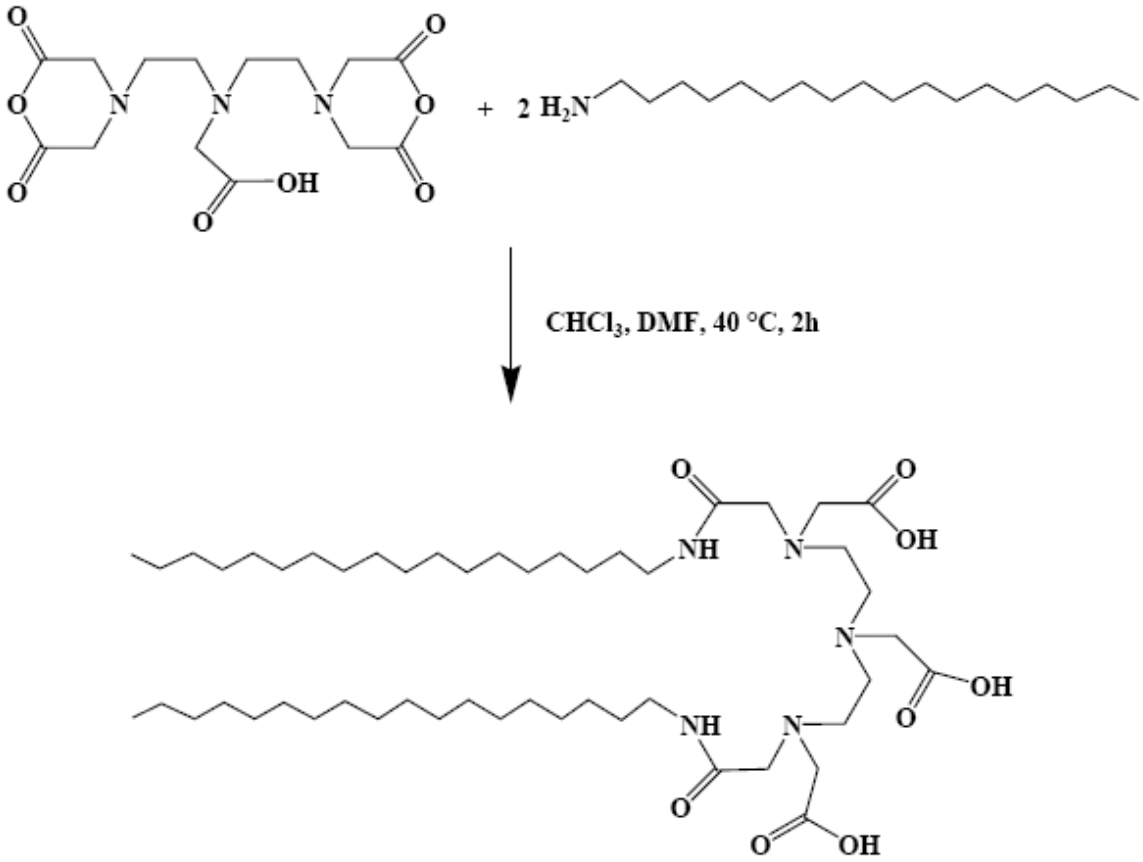

Scheme 4. Synthesis of diethylenetriamine pentaacetic acid bis-stearylamide (DTPA-DSA)

Diethylenetriamine pentaacetic acid (DTPA) dianhydride (1.965 g; 5.5 mmol, Aldrich) was dissolved in 200 ml of anhydrous DMF (ACROS) at 40 °C. Octadecylamine (stearyl amine, SA, Aldrich) (2.695 g; 10 mmol) was dissolved in 250 ml of anhydrous $CHCl_3$ (ACROS) and added dropwise at 40 °C. The reaction mixture was stirred at 40 °C 2h, then cooled down and stored overnight at 4 °C. The white precipitate was filtered off, washed with acetone (0.5 L, Fisher) dried, then heated in boiling absolute ethanol (1 L, Fisher) and filtered hot. The filtrate was cooled down and the precipitate was filtered off and air-dried. The resulting crude product was boiled in chloroform for 3 h. After filtration the solid was stirred in 1 L of boiling water 3h. The dry residue was crystallized from 2 L of absolute ethanol. The white crystals were filtered off and dried under vacuum. Obtained 3.22 g of DTPA-DSA (71.8 %). MALDI-TOF (895 $[M]^+$, 918 $[M+Na]^+$). ^1H NMR (500 MHz, CF_3COOD, 305 K, δ ppm, ref. CF_3COOH, 11.62 ppm): 4.58 (s, 4H, CH_2), 4.56 (s, 4H, CH_2), 4.18 (s, 2H, CH_2), 4.1 (m, 4H, CH_2), 3.8 (m, 4H, CH_2), 3.41 (t, 4H,

CH_2), 1.6 (m, 4H, CH_2), 1.3 (m, 60H, CH_2), 0.9 (t, 6H, CH_3). TLC ($CHCl_3$/MeOH/H_2O/CH_3COOH, 25/15/4/2, v/v) R_f = 0.4.
DTPA-DSA was used for Gd^{3+} loading.

Synthesis of DTPA-DSA-Gd monohydrate.

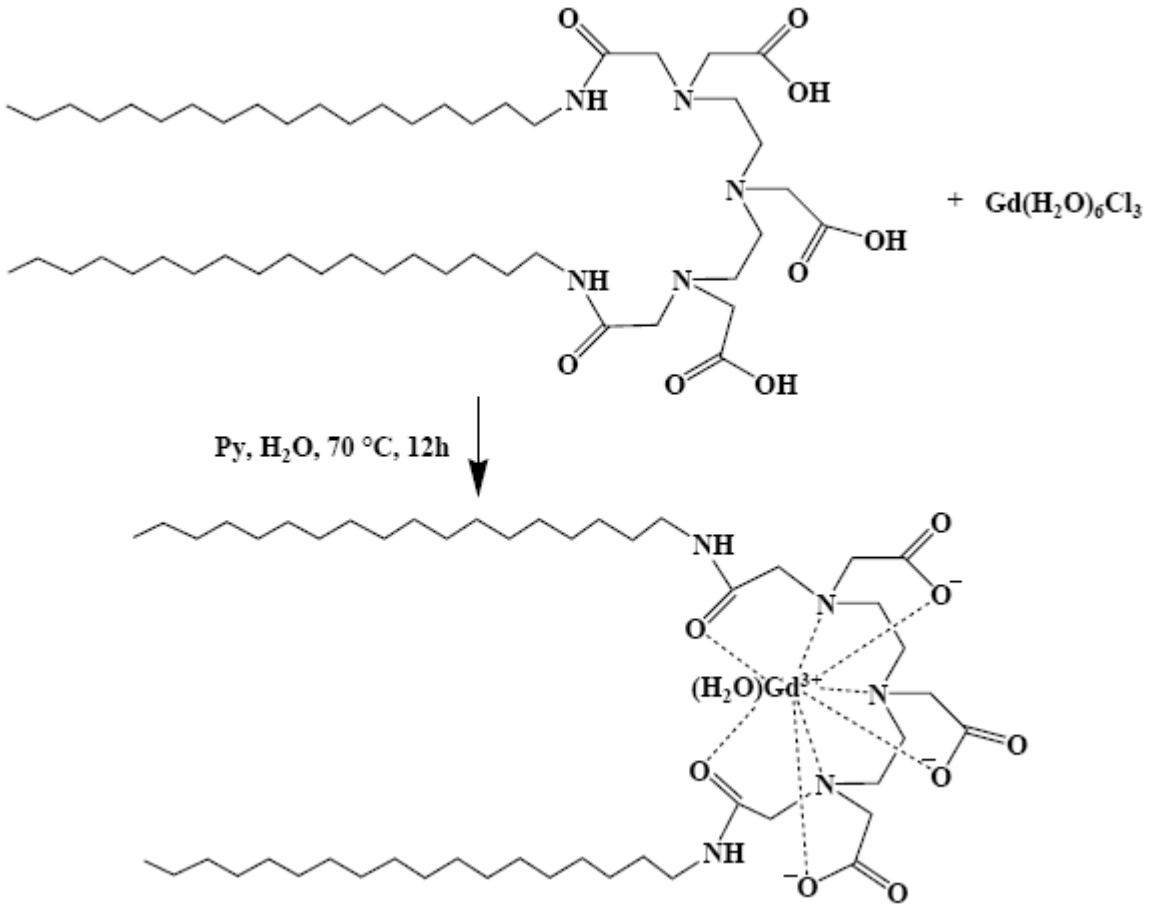

Scheme 5. Synthesis of DTPA-DSA-Gd monohydrate

Gadolinium (III) chloride hexahydrate (408.3 mg 1.1 mmol, Aldrich) was dissolved in water (1 mL) and added to a mixture of DTPA-SA (896.3 mg, 1 mmol) and dry pyridine (30 mL, ACROS). The reaction mixture was stirred overnight at 70 °C. The volatiles were evaporated under reduced pressure. The residue was heated at reflux in ethanol (0.5 L) 1h. Then most of the solvent was evaporated until 100 mL volume and the product was precipitated into water (1 L). The solid greenish crystals were filtered off, washed with water (3x300 mL) and dried in vacuum. The absence of free gadolinium was checked with xylenol orange indicator. Yield 890.1 mg (83.3%). MALDI-TOF 1091 $[M+Na]^+$.
DTPA-DSA-Gd monohydrate is to be incorporated into the lipid nanoparticles shell for MRI and multimodal imaging.

2.2.2. Synthesis of core components

Synthesis of 5-Androsten-17*β*-Boc-amino-3*β*-yl Oleate (BOC-CE-OA, Scheme 6)

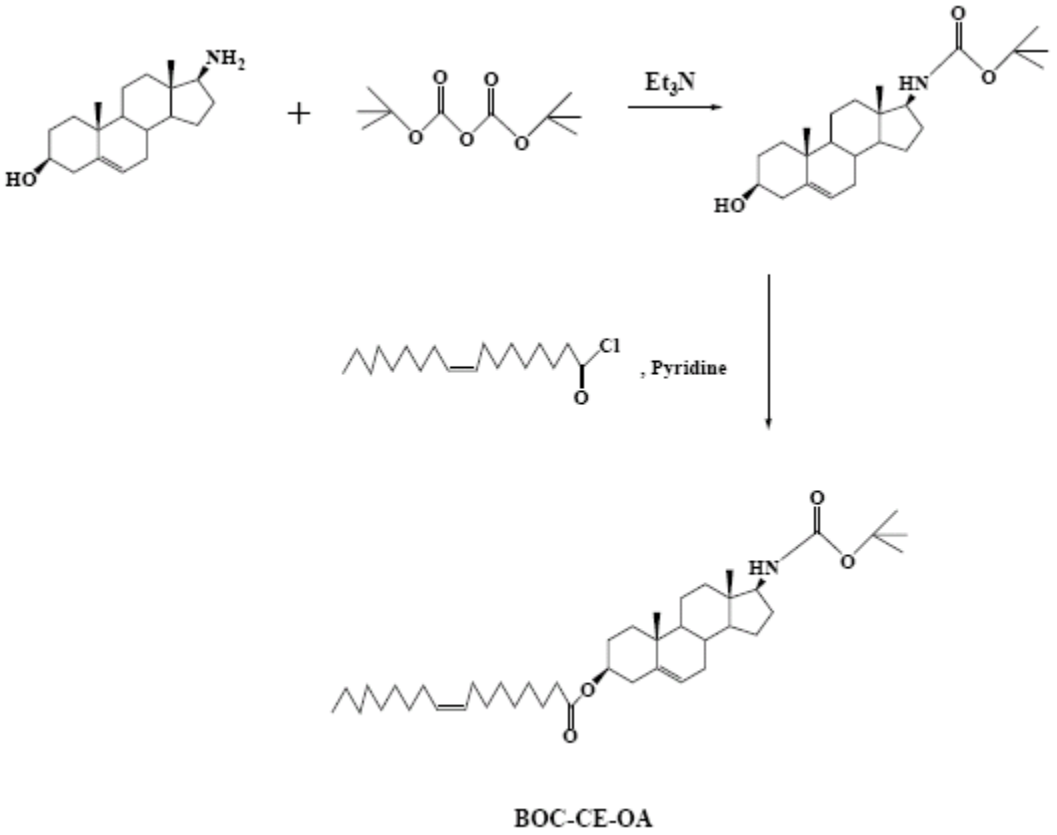

Scheme 6. Synthesis 5-Androsten-17*β*-Boc-amino-3*β*-yl Oleate (BOC-CE-OA)

Synthesis of 5-Androsten-17*β*-Boc-amino-3*β*-ol (BOC-CE)

Di-*tert*-butyl dicarbonate (420 g, 1.90 mmol) was added to a solution containing 5 androsten-17*β* -amino-3*β*-ol (475 mg, 1.64 mmol) and triethylamine (0.27 mL, 1.94 mmol) in dichloromethane (50 mL). The reaction mixture was stirred at room temperature for 2 days. Evaporation of the solvent gave a white residue. This crude product was purified by silica gel column chromatography (30% ethyl acetate in hexanes) to give BOC-CE as a white solid in 95% yield (610 mg, 1.57 mmol). Mp: 168-172 °C; exact mass calcd: 389.3; found by ESI-MS: 390.4 (MH+). Anal. Calcd for $C_{24}H_{39}NO_3$: C, 73.99; H, 10.09; N, 3.60. Found: C, 73.52; H, 10.39; N, 3.19. ^{1}H NMR ($CDCl_3$): δ 5.34 (m, 1H, 6-H), 4.42 (brs, 1H, N-H), 3.53 (m, 2H, 3-H + 17-H), 2.27 (m, 2H), 2.17-1.92 (m, 2H), 1.90-1.70 (m, 3H), 1.69-1.49 (m, 6H), 1.48-1.32 (m, 3H), 1.44 (s, 9H for *tert*-butyl), 1.31-1.15 (m, 2H), 1.15-0.95 (m, 2H), 1.00 (s, 3H, 19- CH_3), 0.67 (s, 3H, 18-CH_3); ^{13}C NMR ($CDCl_3$): δ 156.2, 141.1, 121.5, 79.2, 71.9, 60.5, 53.0, 50.4, 42.8, 42.5, 37.5, 37.2, 36.8, 32.3, 31.8, 31.7, 29.0, 28.6, 28.6, 28.6, 23.7, 20.9, 19.6, 12.0.

Synthesis of 5-Androsten-17*β*-Boc-amino-3*β*-yl Oleate (BOC-CE-OA)

Oleoyl chloride (710 mg, 2.35 mmol) was slowly added into a 20 mL pyridine solution of BOC-CE (610 mg, 1.57 mmol). After 2 h, the reaction mixture was poured into 40 mL of icewater. It was filtered and washed with water three times to give a crude residue. This crude product was then chromatographed on silica column with 10% ethyl acetate in hexanes to afford the title compound as sticky solid in 60% yield (615 mg, 0.94 mmol). Exact mass calcd: 653.5; found by ESI-MS: 654.6 (MH^+). Anal. Calcd for $C_{42}H_{71}NO_4$: C, 77.13; H, 10.94; N, 2.14. Found: C, 77.35; H, 11.41; N, 1.76. 1H NMR ($CDCl_3$): δ 5.32 (m, 3H, 6-H + 2 x vinyl-H of oleate), 4.58 (m, 1H, 3-H), 4.41 (brs, 1H, N-H), 3.52 (m, 1H, 17-H), 2.28 (m, 4H), 2.17-1.70 (m, 10H), 1.61 (m, 8H), 1.50-1.38 (m, 2H), 1.43 (s, 9H for *tert*-butyl), 1.37-0.95 (m, 23H), 1.00 (s, 3H, 19-CH_3), 0.85 (t, 3H, terminal CH_3 of oleate), 0.65 (s, 3H, 18-CH_3); ^{13}C NMR ($CDCl_3$): δ 173.3, 139.4, 130.1, 129.9, 122.4, 78.1, 73.7, 60.5, 52.8, 50.2, 42.7, 38.3, 37.1, 37.0, 36.8, 34.8, 32.2, 32.1, 31.7, 29.9, 29.8, 29.7, 29.5, 29.5, 29.3, 29.3, 29.2, 29.2, 28.9, 28.6, 28.6, 28.6, 27.9, 27.4, 27.3, 25.2, 23.7, 22.8, 20.7, 19.5, 14.3, 11.9.

2.2.3. Assembling the nanoparticles

To assemble nanoparticles, we combined chloroform solutions of PEGylated lipids (1,2-distearoyl-*sn*-glycero-3-phosphoethanolamine-N-[methoxy(polyethylene glycol)-1000]), metal-chelating lipids (1,2-dioleoyl-*sn*-glycero-3-[(N-(5-amino-1-carboxypentyl)iminodiacetic acid)succinyl]), cholesterol esters and lipids conjugated with imaging agents. Excess of the PEGylated lipids (70-80%) provided the formation of lipid monolayer shell to avoid creation of a bilayer shell that would significantly increase the size of the lipid particles. 20% of DOGS-NTA containing lipids allowed to maximize the density of metal chelating groups and, consequently, the density of ligands bound to the nanoparticles and the strength of His_6-tagged ligand interaction with the metal chelating groups[8]. 10-15% of cholesterol esters were sufficient to completely fill out the interior space of the nanoparticles that served as the nanoparticles core. When the content of the core lipids was increased the lipid precipitation was observed indicating that nanoparticle core can accommodate a limited amount of cholesterol esters molecules.
Chloroform was removed with argon stream and lipid film additionally dried under vacuum for 3hr. Lipids were hydrated under argon with hot (65-80 $^{\circ}$C) HBS buffer (10 mM HEPES, 140 mM NaCl) by intermitted vortex and were cooled down in a water bath to room temperature. Micelle suspension was filtrated through a 0.2 μm mini filter (Sterlitech) and kept under argon at 4 $^{\circ}$C.

2.2.4. The nanoparticle size measurements

To vary the particles size we used core lipids of different nature. The nanoparticles without core were used as control. The size of the resulting nanoparticles was determined by dynamic light scattering (Table 1 and Fig.1). The particles with cholesterol core had largest size (up to 20 nm) due to cholesterol molecule intercalation between the shell lipids. After addition of fatty acid moiety to cholesterol molecule the nanoparticles size was decreased due to strong hydrophobic interaction between core molecules. Nanoparticles containing cholesterol ester derivatives that formed intermolecular hydrogen bonds had a smallest size, which approximately equal to the size of antibodies, with narrow size distribution pattern.

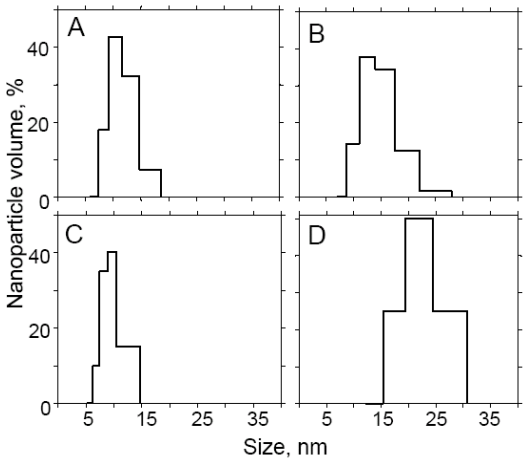

Figure 1. *Size distribution of nanoparticles from Dynamic Light Scattering analysis (A, B, C, D – see Table 1)*

Table 1. Dependence of the lipid nanoparticles size on the core content

Name of nanoparticles	PEGylated lipid, %	Ni-NTA lipid, %	Core lipid, name and %	Size, nm
A	78	22	N/A	10.1±5.4
B	70	20	10 (cholesterol ester) 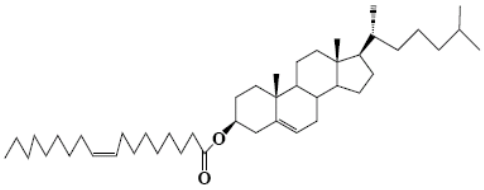	12.8±7.3
C	70	20	10 (BOC-CE-OA) 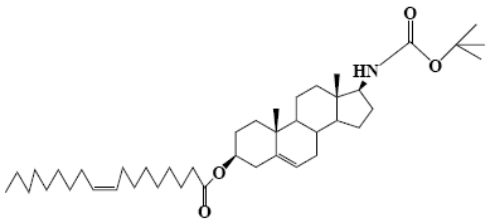	8.4±3.4
D	70	20	10 (cholesterol) 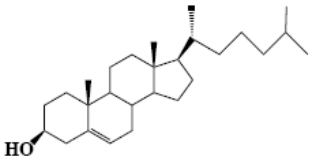	19.7±9.1

2.2.5. Formation of fluorescent nanoparticles

To endow lipid nanoparticles with fluorescent properties the porphyrin-based fluorophore, i.e. pyropheophorbide *a* was utilized. The pyropheophorbide *a* is excited by near infrared light that easily penetrates into live tissues and can be used for imaging and killing of breast cancer cells *in vivo*. To make fluorescently labeled lipid nanoparticles we used two different strategies: lipid-conjugated fluorochrome was introduced into either core or shell lipids of the nanoparticles. Pyro-CE-OA that contains cholesterol oleate moiety has been included in the nanoparticle core while pyropheophorbide *a* conjugated with phosphatidylethanolamine (Pyro-PE) have been incorporated into the shell.

Before the assembly of the nanoparticles each fluorescent conjugate was dissolved in chloroform, and absorption of the solution was measured at 410 nm. Using the extinction coefficient for Pyro that was determined as we described early (ε = 110,000 $M^{-1}cm^{-1}$)[7] we were able to calculate the concentration of the Pyro conjugate solutions. To avoid self-quenching process we included only 3 mol% of flluorochrome molecules into the nanoparticle. To core formation we used acylated amino-cholesterol (BOC-CE-OA) ester, that formed smallest NP (diameter 8 nm, Fig. 1, Tab. 1). For comparison reasons, we have also utilized DiI (Invitrogen), a lipophilic analog of an FDA approved carbocyanine dye, that was introduced into the lipid shell.

2.2.6. Functionalization of the nanoparticles with His_6-tagged protein

Elevated expression of cell surface receptors such as HER-2/neu[9-16] or integrin αvβ3 or α5β1 have been noted on breast cancer cells that is essential to tumorigenesis[17]. Every so often intrinsic affinity of receptor to natural ligands or peptidomimetics is relatively low (≈ 10^4 L/M). Nevertheless we expect strong multivalent binding of the nanoparticles carrying ligands the specific receptors on breast cancer cells according to our previous data[18]. To test this hypothesis we used a model cell-nanoparticle system, which consists from nanoparticles functionalized with ICAM-1 ligand that recognized αLβ2 integrin and CER-43 human T cell line over-expressing the latter molecule on the cell surface. We expressed soluble recombinant ICAM-1 protein containing His_6-tag on the C-end of the molecule in Drosophila cell system and purified by affinity chromatography on monoclonal antibody against human ICAM-1 (HB9580, ATCC) (data not shown).

The nanoparticles functionalization included two steps. (i) To load NTA-DOGS shell lipids with Ni^{2+} a Bio-Rad mini column with cut off 6 kDa was equilibrated with 100 mM $NiSO_4$, and the nanoparticles solution at total lipid concentration of 5 mM was passed through the column to exchange the buffer. After 30 min of incubation unbound Ni^{2+} ions were removed by an additional cycle of gel filtration on the Bio-Rad mini column pre-equilibrated with HBS buffer. (ii) The resulting nanoparticles containing imaging agent (see section 2.2.5.) at total lipid concentration around 5 mM were mixed with equal volume of the His_6-tagged recombinant ICAM-1 at different concentrations (up to 100 μM). The mixture was incubated at room temperature during 10 min and desirable amount of PBS with 1% BSA was added.

2.2.7. Analysis of the nanoparticle specificity by Flow Cytometry

To analyze binding specificity of ICAM-1-NPs two different NPs were used: (i) NP containing fluorescent lipid conjugate in the core (ICAM-1-NP-Pyro-CE-OA) and (ii) NP with fluorescent lipids in the shell (ICAM-1-NP-Pyro-PE). The NP were added to CER-43 cells in PBS buffer containing 1mM Ca^{2+}, 1 mM Mg^{2+} and 1% BSA. About 10 nmol lipid was used per 200,000 cells. Control cells were stained with unloaded particles. The cells were incubated for 3hr at 37°C, washed free of unreacted reagents and analyzed by Flow Cytometry. As shown in **Figure 2A** and **B** the loaded nanoparticles specifically stain CER43 cells without significant background. The cells incubated with ICAM-1-NP-Pyro-PE stained more intensely (higher MFI) than ICAM-1-NP-Pyro-CE-OA treated cells.

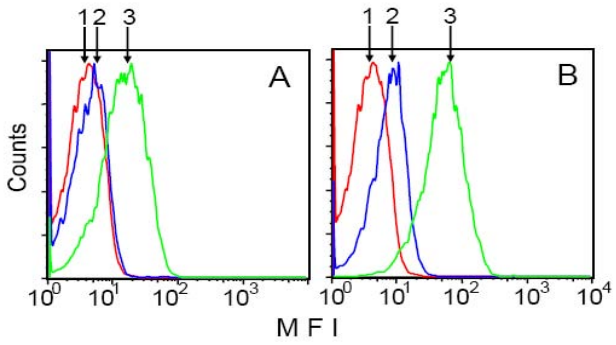

Figure 2. *Binding of ICAM-1-NP (3) to CER-43 cells expressing alphaLbeta2 integrins on the surface that specifically recognize ICAM-1 molecule: (**A**) ICAM-1-NP-Pyro-CE-OA and (**B**) ICAM-1-NP-Pyro-PE. Untreated cells (1) and cells incubated with plain NP, i.e., untargeted nanoparticles (2) were used as negative controls. Fluorescence was excited at 633 nm and emission was collected at 675 nm.*

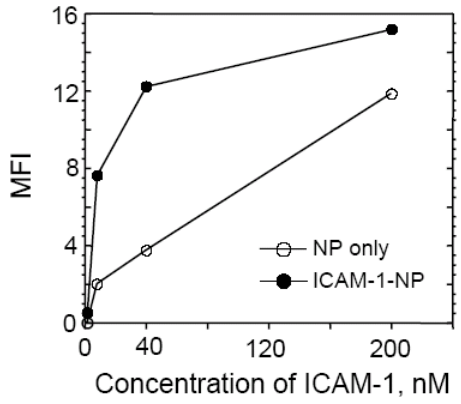

Figure 3. *The binding of ICAM-1-NP-Pyro-CE-OA to CER-43 cells upon concentration of ICAM-1 is shown. Cells incubated with untargeted nanoparticles were used as a negative control.*

The staining was highly sensitive ($K_{avidity}$ ~ 8 nM) presumably due to multivalent nature of ICAM-1-NP (**Fig. 3**).

To understand better the difference in the staining pattern of NP containing different fluorescent conjugates we investigated changes of the cell MFI as function of time (**Fig. 4A** and **B**). As clearly evident from **Figure 4** the fluorescence of the cells stained with ICAM-1-NP-Pyro-PE dramatically increased while fluorescence of the cells incubated with ICAM-1-NP-Pyro-CE-OA stayed constant. We suggest that shell-associated fluorescent lipids can exchange with cell membrane lipids allowing accumulation of fluorochrome in the cell membrane of target cells thus increasing intensity of cell staining[19]. Pyro-CE-OA conjugate lipids have much lower ability to accumulate in the cell membrane. Moreover, after releasing content of endocytosed NP in cytoplasm Pyro-CE-OA conjugate lipids can aggregate limiting cell fluorescence due to self-quenching.

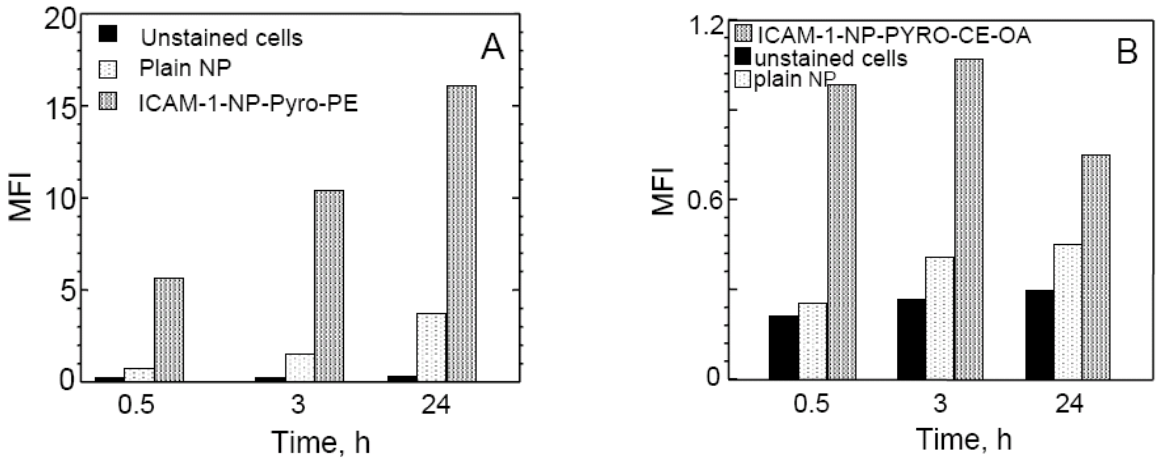

Figure 4. *Time course of the cell staining using different ICAM-1-NP is shown. CER-43 cells were incubated in the presence of ICAM-1-NP-Pyro-PE (**A**) or ICAM-1-NP-Pyro-CE-OA (**B**) for 30 min to 24 h. After repeated washing to remove free nanoparticles the cells were analyzed by Flow Cytometry.*

2.2.8. Fluorescent image analysis

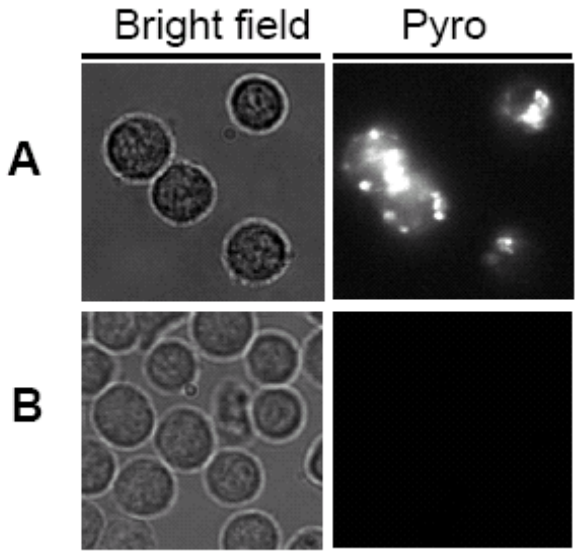

Figure 5. *Binding of ICAM-1-NP-Pyro-PE to the surface of live cells. CER-43 cells were stained with ICAM-1-NP-Pyro-PE for 3 hr at 37 °C. Plain NPs were used as a negative control. About 10 nmol of lipids was used per 200,000 cells. After washing procedure the samples were used for microscopy on a traditional wide field fluorescence microscope with Live Cell System. The probes near-infrared fluorescence were excited by Xenon Lamp at 620/60 nm and emission was collected with 700/75 nm band pass filter.*

The specificity of the ICAM-1-NP-Pyro-PE binding was also evident from the analysis of fluorescence images of CER-43 cells incubated with the NPs at 37 °C (**Fig. 5**). The binding of untargeted NPs to the CER-43 cells was not observed thus confirming specificity of the process (**Fig 5B**). Interaction of ICAM-1-NP-Pyro-PE with the surface of CER-43 cells leads to internalization of the NPs that is evident from punctate surface and intracellular staining (**Fig 5A**). The intensity of the staining and amount of internalized NP increased with time (data not shown). Thus, the imaging data confirm the NP targeting at the cell surface and subsequent receptor mediated uptake.
To support the above data we used ICAM-1-NP loaded with well-characterized lipophilic tracer DiI.

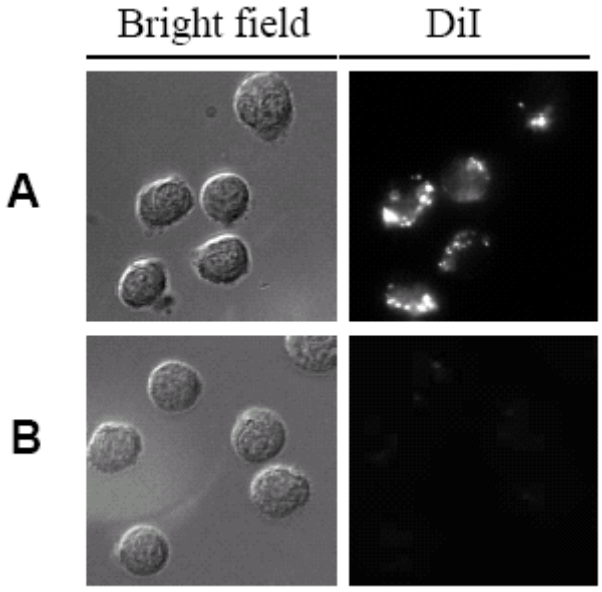

Figure 6. *CER-43 cells staining with DiI loaded ICAM-1-NP. CER-43 cells were stained with ICAM-1-NP-DiI as described in Figure 5. Samples were exited at 540/20 nm and emission was collected with D605/55 nm filter.*

It is weakly fluorescent in aqueous environment. However, it is highly fluorescent when incorporated into lipid membranes such as plasma, endosome and lysosome membranes. After incubation of the CER-43 cells with ICAM-1-NP-DiI the staining pattern, i.e., intensity, specificity and localization of the fluorescent probe, was similar to the fluorescence of the ICAM-1-NP-Pyro-PE treated cells (**Fig. 6**).

3. Key Research Accomplishments:

We have successfully synthesized two fluorescent lipid conjugates that suitable for NIR imaging: (i) pyropheophorbide *a* with phosphatidylethanolamine and (ii) pyropheophorbide *a* with cholesterol oleate. We have also synthesized a lipid DTPA-Gd derivative for MRI and the nanoparticles core building block – an acylated cholesterolamine oleate.
We have assembled four different nanoparticles with core of different nature that affect on nanoparticles average size (from 8 nm for the smallest nanoparticles to 19 nm for the largest nanoparticles).
We have fabricated two kinds of fluorescent nanoparticles containing fluorescent lipids either in the core or in the shell. We have conjugated the nanoparticles with the integrin ligands.
We have showed the specificity and measured sensitivity of the conjugated fluorescent nanoparticles using *in vitro* model system.
We are currently arranging the experiments to conjugate the nanoparticles with anti-HER-2/neu affibodies[20] and AHNP peptidomimetic of the anti-HER-2 rhu mAb 4D5[21] (Masuda K., Richter M., Song X., et. Al. AHNP-streptavidin: a tetrameric bacterially produced antibody surrogate fusion protein against $p185^{her2/new}$. Oncogene 2006; 25:7740-7746).
The agents that are used to conjugation have low molecular weight and activity from submicromolar to picomolar range. To attach the AHNP to the nanoparticle Ni-NTA chelate we have connected the peptidomimetic (FCDGFYACYMDV) with His_6-tag using a flexible linker GGGGSRSNSSS. The affibodies, which containe C-terminal cysteine, are conjugated with the nanoparicles that included functionalized PEG lipid (DSPE-PEG(2000) Maleimide, Avanti Polar Lipids, Inc).
The conjugates binding specificity and sensitivity to HER-2/neu will be measured using two breast cancer cell lines, SK-BR-3 and MDA-MB-468 that expressed profoundly different amount of the HER-2/neu on the cell surface. The stability of the nanoparticles in serum containing media will be also measured.

4. Reportable Outcomes:

1. A.V. Popov. “Developing Molecular Probes and Nanoparticles for Imaging”. University of Pennsylvania. March 5, 2009. Seminar for Research Assistant Professor position application.
2. Nadia Anikeeva, Yuri Sykulev, E. James Delikatny, and Anatoliy V. Popov. (2009) “Lipid-Based Nanoparticles for Targeted Delivery of Imaging Agents into Breast Cancer Cells and Cytotoxic T lymphocytes.” The 3rd International Congress of Nanobiotechnology & Nanomedicine in San Francisco, June 22-24, 2009 Session Abstracts & Proceedings Table of Contents, T-A-6 AB PR. (Oral presentation, speaker A.V. Popov).
3. A.V. Popov, T.M. Mawn, S. Kim, G. Zheng, and E.J. Delikatny. “Design and Synthesis of Phospholipases C and A_2-Sensitive Self Quenched Near Infrared Fluorescent Smart Probes”. J. Amer. Chem. Soc. (In preparation)

5. Conclusions:

We have successfully been able to produce lipid-based targeted nanoparticles suitable for NIR imaging. This approach permits rapid generation of the targeted nanoparticles with different properties. Moreover, the excitation of chlorophyll-based fluorophores produce singlet oxygen species that causes death of the targeted tumor cells, a basis for photodynamic therapy (PDT).

6. References:

1 Alexis, F., Rhee, J.-W., Richie, J. P., Radovic-Moreno, A. F., Langer, R. & Farokhzad, O. C. New frontiers in nanotechnology for cancer treatment. *Urol. Oncol.: Semin. Orig. Invest.* **26**, 74-85 (2008).

2 Cho, K., Wang, X., Nie, S., Chen, Z. & Shin, D. M. Therapeutic Nanoparticles for Drug Delivery in Cancer. *Clin. Cancer Res.* **14**, 1310-1316 (2008).

3 Torchilin, V. P. PEG-based micelles as carriers of contrast agents for different imaging modalities. *Adv. Drug Delivery Rev.* **54**, 235-252 (2002).

4 Allen, T. M. Ligand-targeted therapeutics in anticancer therapy. *Nat. Rev. Cancer* **2**, 750-763 (2002).

5 Bawarski, W. E., Chidlowsky, E., Bharali, D. J. & Mousa, S. A. Emerging nanopharmaceuticals. *Nanomedicine* **4**, 273-282. (2008).

6 Heikela, M., Vattulainen, I. & Hyvonen, M. T. Atomistic simulation studies of cholesteryl oleates: model for the core of lipoprotein particles. *Biophys. J.* **90**, 2247-2257 (2006).

7 Popov, A. V., Mawn, T. M., Kim, S., Zheng, G. & Delikatny, E. J. Design and Synthesis of Phospholipases C and A_2 -Sensitive Self Quenched Near Infrared Fluorescent Smart Probes. *J. Am. Chem. Soc.*, (In preparation).

8 Anikeeva, N., Mareeva, T., Liu, W. & Sykulev, Y. Can oligomeric T-cell receptor be used as a tool to detect viral peptide epitopes on infected cells? *Clin. Immunol. (Amsterdam, Neth.)* **130**, 98-109 (2009).

9 Ciampa, A. & Khan, A. HER-2/neu status in breast cancer: "to FISH or not to FISH". *Recent Res. Dev. Hum. Pathol.* **1**, 229-236 (2003).

10 Dhesy-Thind, B., Pritchard, K. I., Messersmith, H., O'Malley, F., Elavathil, L. & Trudeau, M. HER2/neu in systemic therapy for women with breast cancer: a systematic review. *Breast Cancer Res. Treat.* **109**, 209-229 (2008).

11 Estevez, L. G. & Seidman, A. D. HER2-positive breast cancer: incidence, prognosis, and treatment options. *Am. J. Cancer (Auckland, N. Z.)* **2**, 169-179 (2003).

12 Ferretti, G., Felici, A., Papaldo, P., Fabi, A. & Cognetti, F. HER2/neu role in breast cancer: from a prognostic foe to a predictive friend. *Curr Opin Obstet Gynecol* **19**, 56-62. (2007).

13 Lipton, A., Demers, L., Leitzel, K., Ali, S. M., Neumann, R., Price, C. P. & Carney, W. P. Circulating HER2/neu: clinical utility. *Biomarkers Breast Cancer*, 235-265 (2006).

14 Meric, F., Hung, M.-C., Hortobagyi Gabriel, N. & Hunt Kelly, K. HER2/neu in the management of invasive breast cancer. *J Am Coll Surg* **194**, 488-501. (2002).

15 Roh, H., Pippin, J. A., Green, D. W., Boswell, C. B., Hirose, C. T., Mokadam, N. & Drebin, J. A. HER2/neu antisense targeting of human breast carcinoma. *Oncogene* **19**, 6138-6143. (2000).
16 Vadgama, J., Wu, Y. & Mehta, M. HER2/neu over expression in breast cancer: methods of detection and therapeutic implications. *Mol. Cell. Pathol. Cancer Prog. Prognosis*, 327-358 (2006).
17 Liapis, H., Flath, A. & Kitazawa, S. Integrin alpha V beta 3 expression by bone-residing breast cancer metastases. *Diagn Mol Pathol* **5**, 127-135. (1996).
18 Anikeeva, N., Lebedeva, T., Clapp, A. R., Goldman, E. R., Dustin, M. L., Mattoussi, H. & Sykulev, Y. Quantum dot/peptide-MHC biosensors reveal strong CD8-dependent cooperation between self and viral antigens that augment the T cell response. *Proc. Natl. Acad. Sci. U. S. A.* **103**, 16846-16851 (2006).
19 Park, J. S., Han, T. H., Lee, K. Y., Han, S. S., Hwang, J. J., Moon, D. H., Kim, S. Y. & Cho, Y. W. N-acetyl histidine-conjugated glycol chitosan self-assembled nanoparticles for intracytoplasmic delivery of drugs: Endocytosis, exocytosis and drug release. *J. Controlled Release* **115**, 37-45 (2006).
20 Tolmachev, V., Orlova, A., Nilsson, F. Y., Feldwisch, J., Wennborg, A. & Abrahmsen, L. Affibody molecules: potential for in vivo imaging of molecular targets for cancer therapy. *Expert Opin. Biol. Ther.* **7**, 555-568 (2007).
21 Masuda, K., Richter, M., Song, X., Berezov, A., Masuda, K., Murali, R., Greene, M. I. & Zhang, H. AHNP-streptavidin: A tetrameric bacterially produced antibody surrogate fusion protein against p185her2/neu. *Oncogene* **25**, 7740-7746 (2006).

7. Appendices. N/A